Tuning the physio-chemical properties of ZnO nanoparticles through annealing process and their photocatalytic activity for dye degradation

C Sridevi (sriphysics1@gmail.com)
Sri Sarada College for Women

A. Suguna
S. Prabhu
M. Geerthana
A. Silambarasan
R. Ramesh
C. Sridevi

Research Article

Keywords: Quasi sphere-like ZnO, Annealing temperature, Methylene blue dye, Hydrothermal method, Photocatalysts

Posted Date: March 17th, 2021

DOI: https://doi.org/10.21203/rs.3.rs-303830/v1

Tuning the physio-chemical properties of ZnO nanoparticles through annealing process and their photocatalytic activity for dye degradation

A. Suguna[a,b], S. Prabhu[b], M. Geerthana[b], A. Silambarasan[c], R. Ramesh[b] and C. Sridevi[d]*

[a]Department of Physics, Shri Sakthikailassh Women's College, Salem, 636 003, Tamil Nadu, India.

[b]Department of Physics, Periyar University, Salem, 636 011, Tamilnadu, India.

Department of Chemistry, Vivekanandha College of Arts and Science for Women, Namakkal, 637211, Tamilnadu, India

dDepartment of Physics, Sri Sarada College for Women, Salem, 636 016, Tamilnadu, India.

*Corresponding Author

C. Sridevi
Assistant professor
Department of Physics
Sri Sarada College for Women
Salem
Tamil Nadu-636 016
India
E-mail: sriphysics1@gmail.com

Abstract

Hexagonal phase zinc oxide nanostructures were synthesized via hydrothermal method and annealed at different temperatures viz., 200, 400, 600, 800 and 1000 °C. The prepared nanostructures were characterized by XRD, FTIR, FESEM, HR-TEM and UV-DRS techniques. The annealing seems to have a profound effect on the crystallinity, morphology and properties of nanostructures. The lattice strain (ε) is calculated from Williamson-Hall (W-H) plot; for nanostructure with small crystallite size the strain is caused by compressive force (intercept is negative) whereas for the large crystallite size tensile force (intercept is positive) determines the lattice strain. The photocatalytic performances were studied by analyzing the degradation of methylene blue (MB) in an aqueous solution. ZnO annealed at 1000 °C exhibited better

photocatalytic activity due to enhanced crystallinity, comparatively lower bandgap and high oxygen vacancy. Thus, ZnO nanostructures prepared here provide a potential solution to general wastewater treatment and drinking water purification.

Key words

Quasi sphere-like ZnO; Annealing temperature; Methylene blue dye; Hydrothermal method; Photocatalysts.

1. Introduction

Development of efficient photocatalyst is the need of the hour. Owing to energy crisis and environmental pollution caused by rapid industrialization, the quest for better photocatalysts is getting intensified. Researchers around the globe are working on several photocatalysts, especially on various metal oxide compounds. Intervening the above research, ZnO is found to be a vital photocatalyst, despite its low chemical stability. Being an amphoteric oxide, ZnO possess good stability near neutral pH, whereas at extreme conditions (Low and high pH), its stability diminishes. ZnO exhibits key scientific and technological advantages such as the efficient charge separation, high photocatalytic activity, simple cost-effective synthetic methods resulting in varied morphological nanostructures, kindled the research towards ZnO nanostructures. However, to make it a commercially viable catalyst, its stability, suppression of charge carrier recombination and light absorption range to be improved [1].

Annealing is a heat treatment pathway often determines the crystal structure, morphology and properties of materials [2]. Numerous reports emphasized the importance of annealing. Kim et al., synthesized ZnO/TiO_2 nanocomposites, found that the photocatalytic activity of the nanocomposites enhanced with increasing annealing temperature of the seed layer from 300°C to 500°C. The high activity of nanocomposites obtained from annealing the seed layer at 500°C was attributed to its high UV absorption ability, large surface area and copious oxygen defects which promoted separation of electron-hole pairs reducing electron recombination [3]. ZnO nanoparticles synthesized by Umar et al., via solution combustion method were subjected to annealing at different temperatures. It was found that the particle size increases from 40 nm to 120 nm with increase in annealing temperature. The ZnO nanoparticles annealed at 600 °C exhibited almost complete photodegradation of the DR-23 dye following a pseudo first order

reaction kinetics [4]. Though the particle size increases with annealing temperature, the activity of photocatalyst is boosted because of its increased native defects, enhanced lifetime of charge carriers and higher quantum yield.

Herein, ZnO nanostructure were synthesized by hydrothermal method, then subjected to annealing at various temperatures, followed by characterization using XRD, UV-DRS, FTIR, FE-SEM and TEM. The photocatalytic activity of ZnO is evaluated by taking methylene blue (MB) as a model pollutant, under UV light.

2. Experimental

2.1. Materials

All the chemicals were of analytical grade and used without any further purification. All solutions were prepared by deionized water. Zinc acetate ($Zn(CH_3COO)_2.2H_2O$) and Methylene Blue ($C_{16}H_{18}ClN_3S$) were purchased from Merck, Dodecylamine **(**$C_{12}H_{27}N$) and Diethylenetriamine ($C_4H_{13}N_3$) were purchased from Hi Media Laboratories Pvt. Ltd.

2.2 Synthesis of ZnO nanoparticles

In the typical experiment, 0.1 mol of zinc acetate dihydrate was dispersed in 80ml of deionized water. The alkaline pH (pH 9- pH 11) is brought down by the addition of surfactants, 5 ml dodecylamine and diethylenetriamine to the above solution under vigorous stirring. After 15 min of stirring, the solution was transferred to Teflon lined stainless steel autoclave, maintained at 200^{o}C in muffle furnace for 15hrs and allow to cool naturally until reaches the room temperature. The resultant product was washed and dried at 80^{o}C for overnight. Further, the product was annealed at 200^{o}C, 400^{o}C, 600^{o}C, 800^{o}C, and 1000^{o}C in a muffle furnace. The obtained samples were characterized by various analytical techniques.

2.3. Characterization

The crystal structure of the samples was characterized using Rigaku X-ray powder diffraction (XRD) with Cu-Kα radiation of wavelength (λ) 0.15418nm. The optical studies were performed using JASCO V-670 double beam spectrophotometer and Bruker NEXUS 470 spectrometer for UV-DRS and FTIR, respectively. The morphology and particle size of the samples were visualized using a field-emission scanning electron microscope (FE-SEM, JEOL JSM-6390LV) and transmission electron microscopy (TEM, Hitachi H-600). The photocatalytic activity of nanoparticles was tested using lab-made photocatalytic reactor, having xenon lamp as UV light source.

2.4 Photocatalytic activity

10 ppm of methylene blue (MB) dye was prepared by dissolving 10 mg of MB in one litre of water. 50 mg of catalyst powder was added to 100 mL of 10 ppm MB solution taken in a specially designed 500 ml photo-reactor with a water circulating unit for cooling. The contents were stirred in dark for 30 min to reach the adsorption and desorption equilibrium using a constant magnetic stirring. After equilibrium, the MB dye with catalyst was irradiated with 400 W xenon lamp with UV filter and the samples were taken at regular interval of 10 min. Nearly, 2 mL of dye solution was pipette-out from the reactor and catalyst particles were separated from the solution by centrifugation at 5000 rpm for 5 min. The concentration of the dye solution was determined by measuring absorbance at 664 nm using a UV–Vis spectrophotometer (JASCO V-670). From the absorbance values, degradation efficiency of the catalyst was determined. The degradation efficiency of the dye i.e. % adsorption has been calculated using equation [17].

$$\boldsymbol{Percentage\ photodegradation} = \frac{C_o - C_t}{C_o} \mathbf{x\ 100} \quad \ldots \quad (1)$$

Where $\boldsymbol{C_o}$is the initial concentration of dye before photo irradiation and $\boldsymbol{C_t}$ is the concentration of dye after photo irradiation.

3. Results and discussion

3.1 x-ray diffraction

The XRD patterns of ZnO nanostructures annealed at 200 °C, 400 °C, 600 °C, 800 °C, 1000 °C was as shown in Fig.1. All the annealed nanostructures exhibited wurtzite structure with $P6_3$ mc space group, matches with JCPDS card No. 36-1451 [5–8]. It was found that the position of diffraction pattern varies a little due to change in strain with annealing. With increase in annealing temperature, peak broadening decreases, whereas peak intensity increases [9]. These changes in diffraction pattern are attributed to increased particle size and crystallinity of nanostructures.

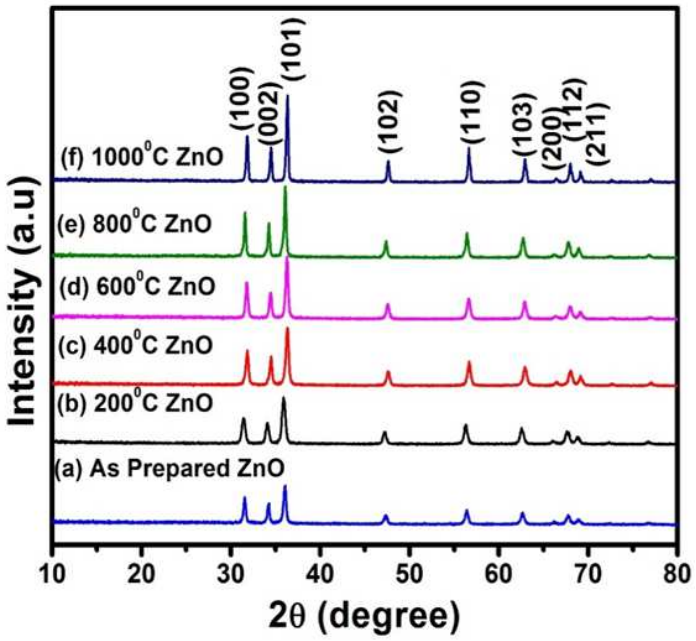

Fig. 1 Powder XRD patterns of (a) ZnO, (b) 200 ºC, (c) 400 ºC, (d) 600 ºC, (e) 800 ºC and 1000 ºC nanostructures.

The average crystallite size of the nanostructures was calculated using Debye-Scherrer formula and Williamson-Hall plot, the values are listed in Table 1. The Debye-Scherrer formula for calculating crystallite size is

$$\boldsymbol{D} = \frac{\boldsymbol{0.94\lambda}}{\boldsymbol{\beta cos\theta}} \ldots (2)$$

Whereas D is the average crystallite size, λ is a x-ray wavelength of Cu kα, β is a full width at half maximum, and θ is a diffraction angle. According to Debye-Scherrer formula, the broadening of XRD peak is due to lowering of crystallite size. But, in actual, two other factors viz., instrumental broadening and lattice strain leads to the broadening of XRD pattern. Assuming the strain induced broadening to be uniform along the crystal, Williamson-Hall equation for the total peak broadening is given by:

$$\beta \cos\theta = 4\varepsilon \sin\theta + \frac{K\lambda}{D} \ldots\ldots\ldots (3)$$

Williamson-Hall plot is constructed by taking 4sinθ along x-axis and βcosθ along y-axis as shown in Fig.2. The obtained plot is linearly fitted. Crystallite size and strain are calculated from the intercept and slope of curve, respectively [10].

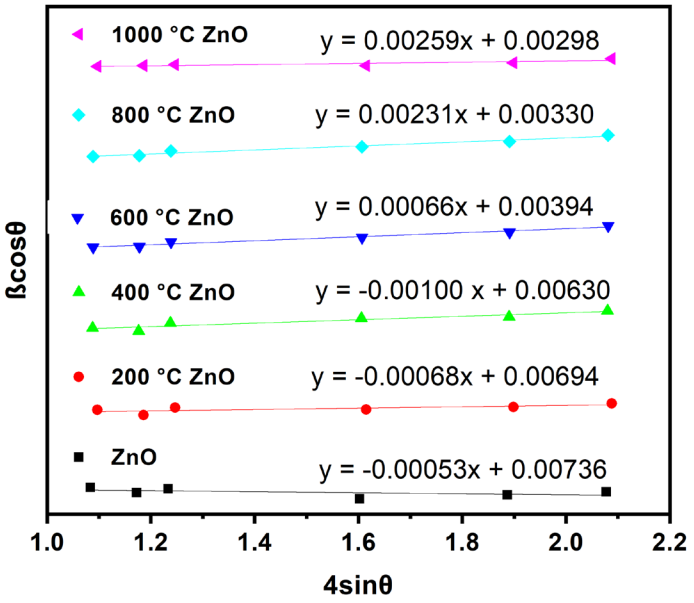

Fig. 2. Williamson–Hall plots for ZnO (as-synthesized) and annealed nanostructures

It is evident from the Fig.3 & Table 1 that the crystallite size of ZnO nanostructures increases with increase in annealing temperature. Apparently, the sign of the lattice strain (ε) is negative for small sized particles whereas the comparatively larger sized particles the sign changes. It is because the crystal lattice will be under the influence of compressive forces, when the lattice strain value is negative and tensile forces will act on the crystal lattice when the strain value is positive.

Table 1. Crystallite size and lattice strain of ZnO nanostructures annealed at various temperatures

Sample	Crystallite size (nm)		Lattic strain (ε) (no unit) $\times 10^{-3}$
	Debye-scherrer formula	W-H Plot	
ZnO	19.7	18.7	0.53
ZnO 200 °C	20.8	19.8	0.68
ZnO 400 °C	18.5	21.8	1.00
ZnO 600 °C	26.4	34.9	0.66
ZnO 800 °C	21.1	41.7	2.31
ZnO 1000 °C	25.4	46.2	2.59

According to Fig. 3 lattice strain changes the sign to positive, when the annealing temperature exceeds 400 °C. Our results are in concurrent with the report of Zak et al.,[11] where crystallite size increases with annealing temperature and crystal is found to under compressive forces, in case of small crystallite size.

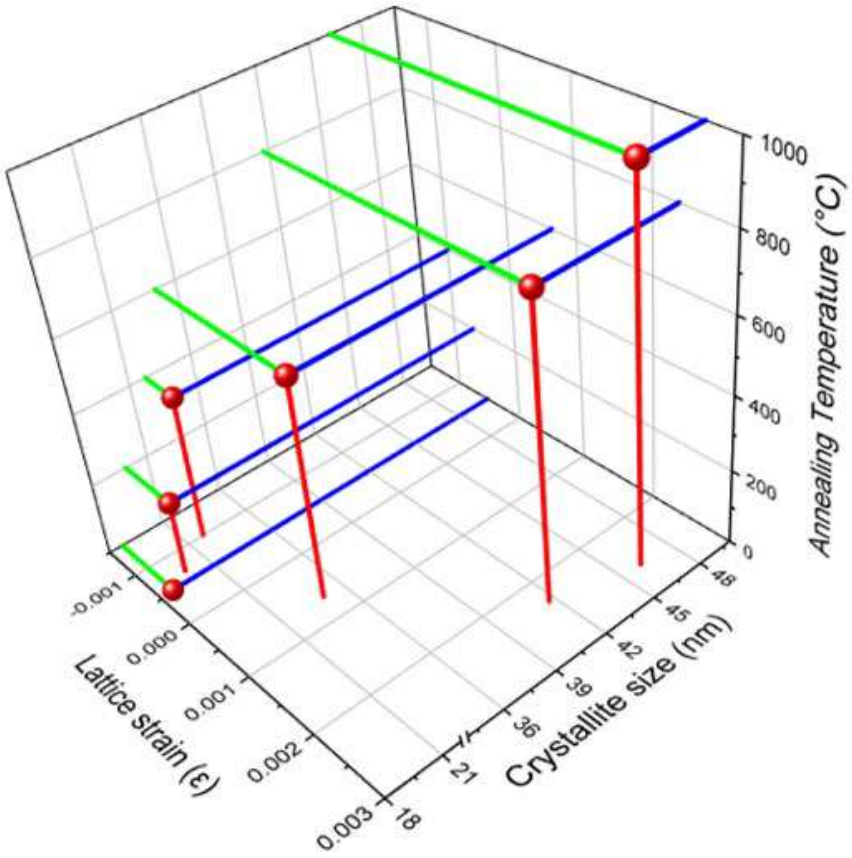

Fig. 3. Plot of lattice strain vs crystallite size and annealing temperature.

3.2 FT-IR analysis

Fig. 4 displays the FTIR spectra of ZnO samples annealed thermally at 200ºC, 400°C, 600°C 800°C, and 1000ºC. The peak at 3340 cm^{-1} and 1630 cm^{-1} represents the fundamental stretching and bending vibration of results from moisture adsorbed at the surfaces [12]. The peaks at the range of 415-520 cm^{-1} are originated to the stretching vibration modes of Zn-O-Zn indicating to the complete transformation from zinc acetate to zinc oxide [13], [14]. The bands at 1300 and 1600 cm^{-1} is assigned to the C-O and C=O stretching modes, whereas, weak absorption bands at 2900 cm^{-1} is attributed to C-H stretching vibration. These vibrations (C-O, C=O, C-H stretching) might have aroused due to the presence of residues from raw materials.

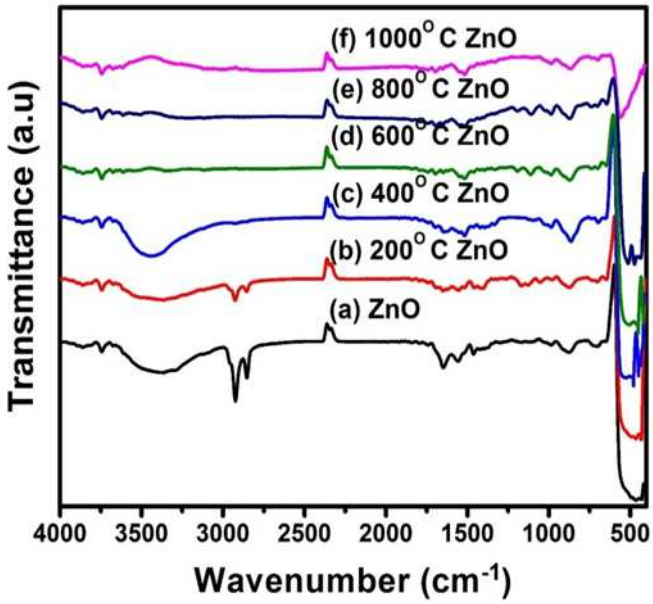

Fig. 4 FTIR spectra of (a) ZnO, (b) 200 ºC, (c) 400 ºC, (d) 600 ºC, (e) 800 ºC and 1000ºC nanostructures.

3.3 FE-SEM analysis

Fig. 5 (a-f) illustrates FE-SEM images of ZnO annealed at different temperatures, it can be seen an appreciable change in the size and morphologies of ZnO. Fig. 5 (a-d) shows, as prepared and ZnO annealed at 400 °C exhibited hierarchical cauliflower-like morphology. The average particle size was found to be around 200 -250 nm. The ZnO annealed at 1000 ºC exhibited quasi spherical shaped nanostructure and the size is calculated to be 300 nm (Fig. 5 (e-f)). On comparing all the FESEM images, it is found that the particle size increased rapidly with increase in annealing temperature. Further, it is noted that hierarchical cauliflower-like nanostructures consist of numerous small sized nanoparticles whereas, quasi spherical shaped nanostructure doesn't seem to have any small particles. Quasi spherical nanostructures might have resulted by the Ostwald ripening mechanism happened during annealing process. In the typical mechanism, bigger particle grown at the expense of smaller particles to form quasi spherical nanostructures. The thermal annealing process proves to be effective in tailoring the morphology and property of ZnO nanostructures.

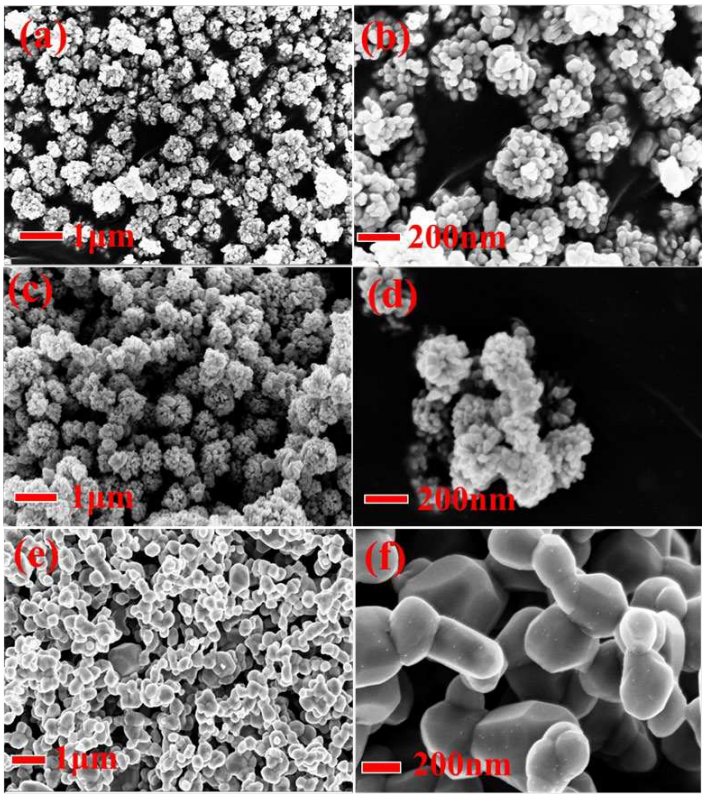

Fig. 5 FE-SEM images for (a-b) as prepared ZnO, (c-d) 400ºC and (e-f) 1000ºC nanostructures.

3.4 TEM and HR-TEM analysis

The internal morphology of the 1000 ºC ZnO samples were studied using TEM and HR-TEM analysis are shown in Fig. 4. The TEM images exhibited quasi spherical ZnO, which is good agreement with the FE-SEM images. The average particles size found to be 300nm for quasi sphere like ZnO. The measured lattice spacing value of 0.27 nm corresponds to the (0001) plane of the ZnO crystal (Fig. 4(b)).

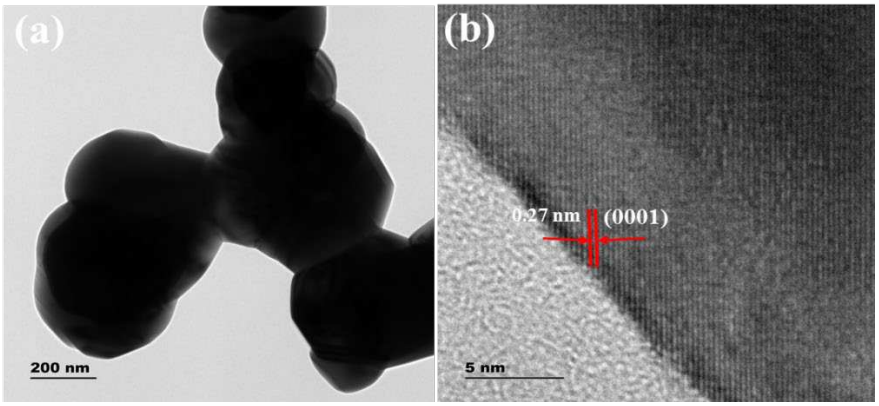

Fig.6(a) TEM and (b) HR-TEM images of 1000°C ZnO nanostructure.

3.5 UV-Vis DRS analysis

The absorbance spectra as synthesized and annealed nanostructures were shown in Fig.7. The UV absorption peak of ZnO ranges from 363 nm to 380 nm. For as-synthesized nanostructures, the absorption peak is at 363 nm and it gradually increases with increasing temperature. The absorption peak is 380 nm for nanostructures annealed to 1000 °C. This shift in absorption peak is attributed to the formation of oxygen vacancies at higher temperature [15]. These oxygen vacancies will aid photocatalytic process for faster degradation organic dye. Based upon the absorbance spectra the optical band gap of the prepared nanoparticles can be calculated from energy and wavelength relation. The decrease in band gap may be due to the influence of various factors such as grain size, structural parameter and carrier concentration [16, 17]. The calculated band gaps were 3.18eV, 3.16eV, 3.15eV, 3.13eV, 3.11eV and 3.10eV for as prepared ZnO, 200^{o}C, 400^{o}C, 600^{o}C, 800^{o}C and 1000^{o}C as shown in Fig. 7(b), respectively.

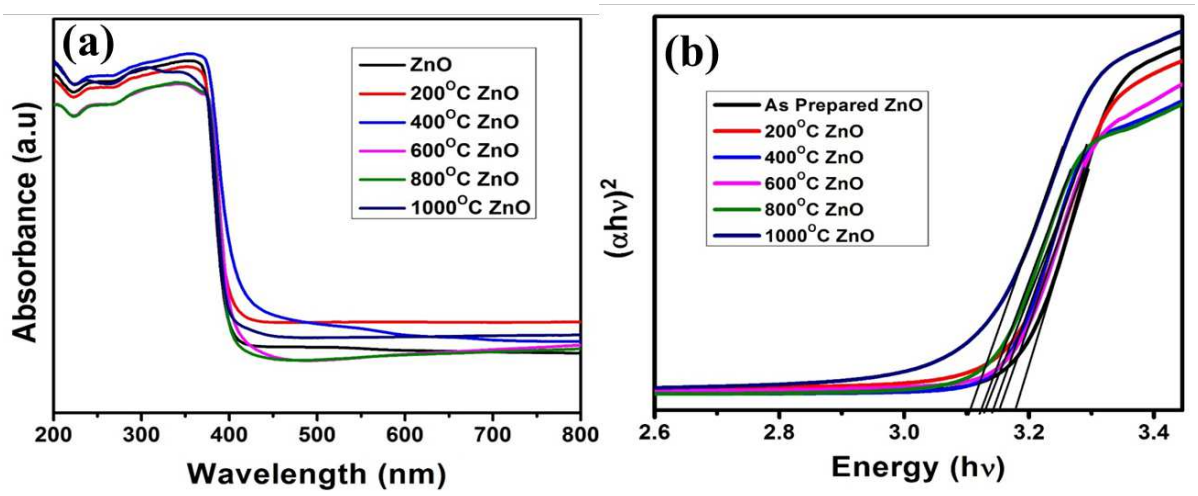

Fig. 7 (a) UV- DRS Spectra and (b) band gap energy of (a) ZnO, (b) 200 ºC, (c) 400 ºC, (d) 600 ºC, (e) 800 ºC and 1000 ºC nanostructures.

3.6. Photocatalytic activities

The photocatalytic performance of the ZnO and annealed ZnO were assessed against the photodegradation of MB dye under UV light irradiation. Fig. 8 shows the MB degradation with as-synthesized ZnO and annealed ZnO nanostructures. It shows the decrease in absorbance intensity of MB dye at regular time intervals. Fig. 9 shows the comparative study of degradation efficiency of as synthesized and annealed nanostructures. From the Fig.7, it is obvious that the

photocatalytic degradation efficiency of nanostructures increases with annealing temperature and ZnO annealed at 1000 °C exhibited better degradation efficiency of 94% in 60 min. From XRD, FESEM and TEM measurements, it is found that the particle size of ZnO increases with increasing annealing temperature. In general, the surface-volume ratio of the larger particles will decrease thereby leading to low photocatalytic efficiency. But, in the present case, though the size of the nanostructures increases, the increase in photocatalytic efficiency might the due to the increased crystallinity of the annealed nanostructures. It is evident from the XRD that the ZnO annealed at 1000 °C displays better crystallinity. High crystallinity of nanostructures, high oxygen vacancy, enhanced the generation and migration of photo-generated charge carriers from bulk to the surface of ZnO nanostructures facilitated the quicker degradation of MB by ZnO annealed at 1000 °C [18, 19]. Recently, Lv et al. reported the ZnO thin film prepared by sol–gel method at different temperature (200 °C–900 °C) and the results indicates the photocatalytic activity of ZnO annealed at 800 °C samples shows higher degradation (88%) of MB within 180 min, this is due to grain size and oxygen deficiency of sample [20].

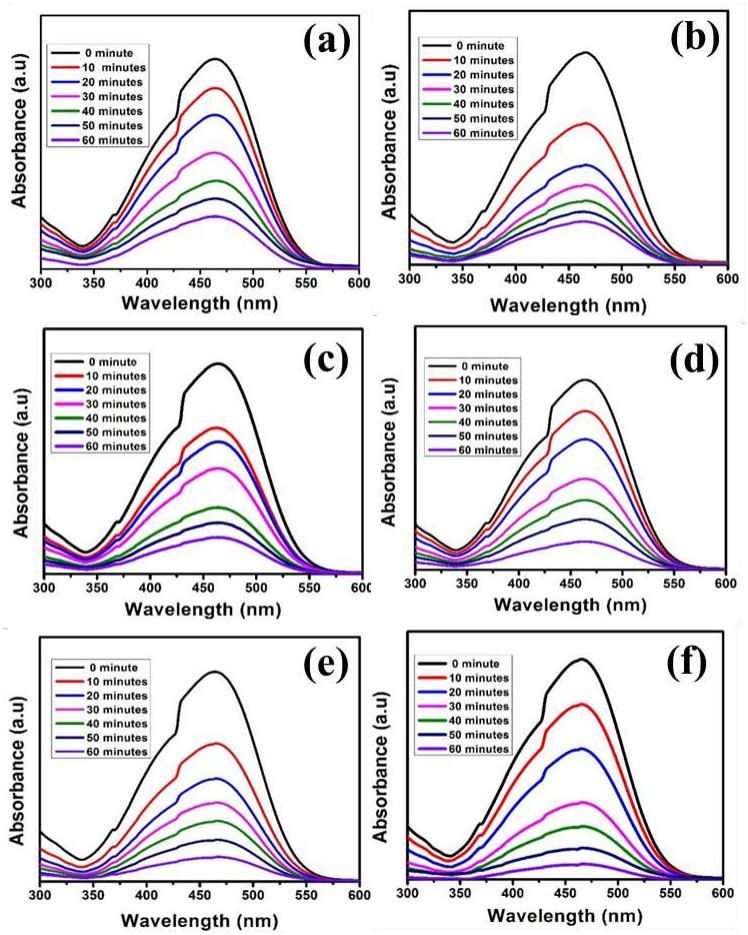

Fig. 8 Photocatalytic activity of ZnO photocatalyst as a function of the irradiation time under different annealing nanoparticles.

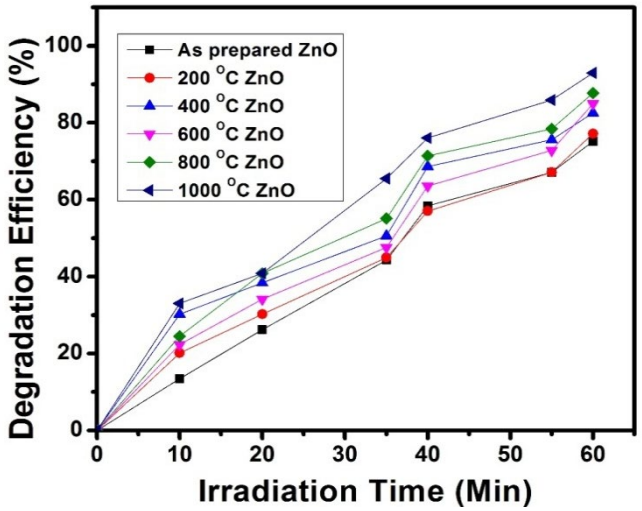

Fig. 9 Degradation efficiency of ZnO photocatalyst as a function of the irradiation time under different annealing nanoparticles.

Photocatalytic Mechanism under UV light

It has been proposed that MB dye molecules are physiosorbed or chemisorbed onto the surface of ZnO nanoparticles where a series of photo induced redox reactions are initiated through the formation of electron/hole pairs (excitones). The optimized band gap of ZnO nanoparticles prevents the formation of electron/hole recombinants [21, 22]. As a result, the conduction band electrons generate various oxygenated free radicals such as •OH through the reduction of chemisorbed O_2 on the surface of the ZnO nanoparticles (Eq. 4-8). Positively charged holes in the valance band are also involved in the formation of •OH free radicals by the ionization and oxidation of water molecules (Eq. 6). The generated •OH radicals are non-selective and strong oxidant which oxidize the aromatic dyes by attacking their aromatic rings and converting them to non-toxic chemical species as shown in the schematic Fig. 10.

$$O_{2+}e_{CB}^{-} \rightarrow O_2^{\cdot -} \quad (4)$$

$$O_2^{\cdot -} + H_2O \rightarrow HO_2^{\cdot} + HO^{-} \quad (5)$$

$$HO_2^{\cdot} + HO_2^{\cdot} \rightarrow H_2O_2 + O_2 \quad (6)$$

$$H_2O_2 + O_2^{\cdot -} \rightarrow HO^{\cdot} + HO^{-} + O_2 \quad (7)$$

$$H_2O + ZnO\ (h_{VB}^{+}) \rightarrow ZnO + HO^{\cdot} \quad (8)$$

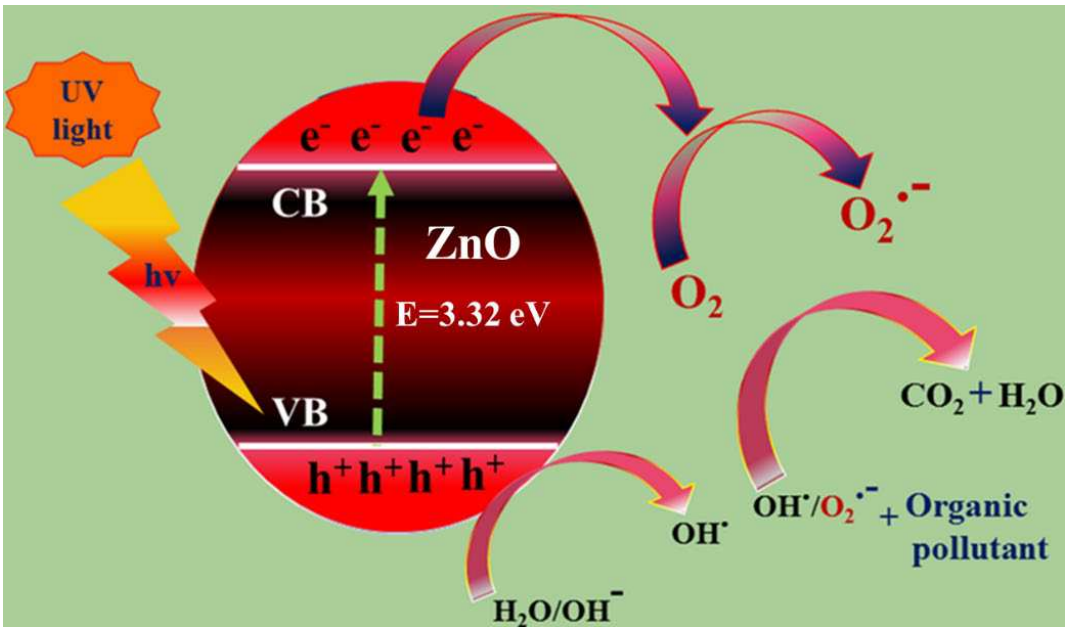

Fig. 8 Schematic diagram of the photocatalytic process for ZnO nanoparticles under UV-light irradiation.

3.7. Recycle test

The stability and reusability properties of the prepared catalyst were investigated by cyclic test (photocatalytic degradation) experiments for ZnO annealed at 1000 ºC against MB dye degradation. From the Fig. 11(A), it is evident that the degradation efficiency of catalyst against MB dye were good upto three cycles [23, 24]. Further, the catalyst was subjected to XRD studies after each cycle and is shown in Fig. 9(B). There is no appreciable change in the diffraction pattern of catalyst. It shows that the catalyst possesses good stability.

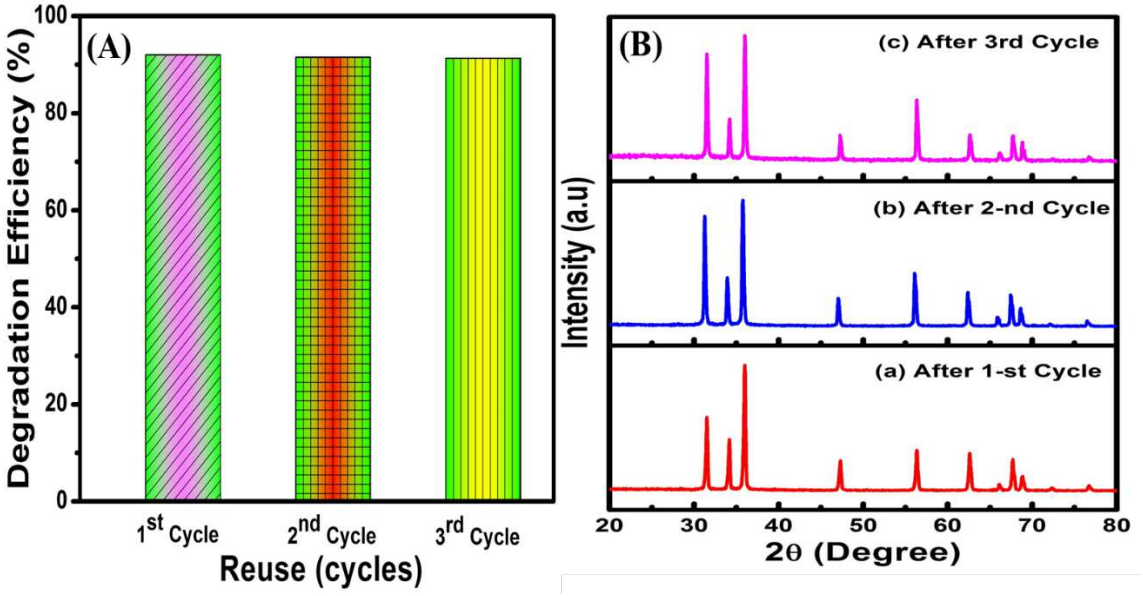

Fig. 11 (A) Reusability test for 1000ºC ZnO photocatalyst up to 3 cycles and (B) XRD patterns of reused 1000ºC ZnO sample up to 3 cycles.

4. Conclusion

ZnO nanostructures synthesized by hydrothermal method were subjected to annealing at various temperatures. The crystallite size of the nanostructures was calculated using Debye-Scherrer and it was compared with W-H plot. For samples with lower annealing temperature, crystallite size from Debye-Scherrer formula is higher, whereas, for samples with higher annealing temperature crystallite size from W-H plot is greater. This is because at lower annealing temperature the lattice strain is caused by compressive force and at higher annealing temperature the lattice stain is due to tensile force. The band gap of ZnO decreases with annealing temperature, and the ZnO nanostructure annealed at 1000 °C exhibits maximum red shift with a band gap of about 3.10 eV. The photodegradation efficiency of ZnO annealed at 1000 °C was approximately

94 percent and a time of 60 minutes under the irradiation of UV light against MB dye. This study offers an eco-friendly and low-cost productivity for the treatment of waste water.

Funding Info

The authors did not receive support from any organization for the submitted work.

Conflict of interest

The authors declare that they have no known competing financial interests or personal relationships that could have appeared to influence the work reported in this paper

Author contribution

Conceptualization: [A.Suguna]; Methodology: [A.Suguna, S. Prabhu and Dr. A. Silambarasan], Formal analysis and investigation: [Dr. C. Sridevi], Writing - original draft preparation: [Dr. C. Sridevi]; Writing - review and editing: [Dr. R. Ramesh], Resources: [A.Suguna], Supervision: [Dr. C. Sridevi].

Animal and Consent to participate (Ethics)

'Not applicable'

References

[1] H. Wu, S. Lin, C. Chen, W. Liang, X. Liu, and H. Yang, “A new ZnO/rGO/polyaniline ternary nanocomposite as photocatalyst with improved photocatalytic activity,” *Mater. Res. Bull.*, vol. 83, pp. 434–441, Nov. 2016, doi: 10.1016/j.materresbull.2016.06.036.

[2] Z. Lu, X. Jiang, B. Zhou, X. Wu, and L. Lu, “Study of effect annealing temperature on the structure, morphology and photocatalytic activity of Si doped TiO 2 thin films deposited by electron beam evaporation,” *Appl. Surf. Sci.*, vol. 257, no. 24, pp. 10715–10720, Oct. 2011, doi: 10.1016/j.apsusc.2011.07.085.

[3] W. Y. Kim, S. W. Kim, D. H. Yoo, E. J. Kim, and S. H. Hahn, “Annealing effect of ZnO seed layer on enhancing photocatalytic activity of ZnO/TiO2 nanostructure,” *Int. J. Photoenergy*, vol. 2013, 2013, doi: 10.1155/2013/130541.

[4] A. Umar, R. Kumar, G. Kumar, H. Algarni, and S. H. Kim, “Effect of annealing temperature on the properties and photocatalytic efficiencies of ZnO nanoparticles,” *J. Alloys Compd.*, vol. 648, pp. 46–52, Jul. 2015, doi: 10.1016/j.jallcom.2015.04.236.

[5] A. Lei, B. Qu, W. Zhou, Y. Wang, Q. Zhang, and B. Zou, “Facile synthesis and enhanced photocatalytic activity of hierarchical porous ZnO microspheres,” *Mater. Lett.*, vol. 66, no. 1, pp. 72–75, Jan. 2012, doi: 10.1016/j.matlet.2011.08.011.

[6] J. B. Zhong, J. Z. Li, Z. H. Xiao, W. Hu, X. B. Zhou, and X. W. Zheng, “Improved photocatalytic performance of ZnO prepared by sol-gel method with the assistance of CTAB,” *Mater. Lett.*, vol. 91, pp. 301–303, Jan. 2013, doi: 10.1016/j.matlet.2012.10.040.

[7] M. V. Vaishampayan, I. S. Mulla, and S. S. Joshi, “Low temperature pH dependent synthesis of flower-like ZnO nanostructures with enhanced photocatalytic activity,” *Mater. Res. Bull.*, vol. 46, no. 5, pp. 771–778, May 2011, doi: 10.1016/j.materresbull.2010.11.007.

[8] H. Wang, S. Dong, Y. Chang, X. Zhou, and X. Hu, “Microstructures and photocatalytic properties of porous ZnO films synthesized by chemical bath deposition method,” *Appl. Surf. Sci.*, vol. 258, no. 10, pp. 4288–4293, Mar. 2012, doi: 10.1016/j.apsusc.2011.12.080.

[9] N. S. Myoung and G. B. Jung, “Effects of annealing temperature and neodymium concentration on structural and photoluminescence properties of Nd3+-doped Y2O3-SiO2 powders,” *J. Rare Earths*, Jun. 2020, doi: 10.1016/j.jre.2020.06.014.

[10] A. Kalita and M. P. C. Kalita, “Williamson-Hall analysis and optical properties of small sized ZnO nanocrystals,” *Phys. E Low-Dimensional Syst. Nanostructures*, vol. 92, pp. 36–40, Aug. 2017, doi:

10.1016/j.physe.2017.05.006.

[11] A. Khorsand Zak, W. H. Abd. Majid, M. E. Abrishami, and R. Yousefi, "X-ray analysis of ZnO nanoparticles by Williamson-Hall and size-strain plot methods," *Solid State Sci.*, vol. 13, no. 1, pp. 251–256, Jan. 2011, doi: 10.1016/j.solidstatesciences.2010.11.024.

[12] N. Srinivasan, M. Revathi, and P. Pachamuthu, "Surface and optical properties of undoped and Cu doped ZnO nanostructures," *Optik (Stuttg).*, vol. 130, pp. 422–426, Feb. 2017, doi: 10.1016/j.ijleo.2016.10.080.

[13] A. Khan, S. N. Khan, and W. M. Jadwisienczak, "One step growth of ZnO nano-tetrapods by simple thermal evaporation process: Structural and optical properties," *Sci. Adv. Mater.*, vol. 2, no. 4, pp. 572–577, Dec. 2010, doi: 10.1166/sam.2010.1127.

[14] Q. Li *et al.*, "Photoluminescence and lasing properties of catalyst-free ZnO nanorod arrays fabricated by pulsed laser deposition," *J. Phys. Chem. C*, vol. 116, no. 3, pp. 2330–2335, Jan. 2012, doi: 10.1021/jp210377s.

[15] J. Yang *et al.*, "Effects of substrate on morphologies and photoluminescence properties of ZnO nanorods," *Appl. Surf. Sci.*, vol. 255, no. 5 PART 1, pp. 2500–2503, Dec. 2008, doi: 10.1016/j.apsusc.2008.07.124.

[16] Y. Liu, A. Liu, W. Liu, Z. Hu, and Y. Sang, "Characterization of optoelectronic properties of the ZnO nanorod array using surface photovoltage technique," *Appl. Surf. Sci.*, vol. 257, no. 4, pp. 1263–1266, Dec. 2010, doi: 10.1016/j.apsusc.2010.08.040.

[17] R. Liu, H. Li, L. Duan, H. Shen, Q. Zhang, and X. Zhao, "Influences of annealing atmosphere on phase transition temperature, optical properties and photocatalytic activities of TiO2 phase-junction microspheres," *J. Alloys Compd.*, vol. 789, pp. 1015–1021, Jun. 2019, doi: 10.1016/j.jallcom.2019.02.198.

[18] N. Charoenthai and N. Yomma, “Effect of annealing temperature and solvent on the physical properties and photocatalytic activity of zinc oxide powder prepared by green synthesis method,” in *Materials Today: Proceedings*, Jan. 2019, vol. 17, pp. 1386–1395, doi: 10.1016/j.matpr.2019.06.159.

[19] F. He, F. Ma, J. Li, T. Li, and G. Li, “Effect of calcination temperature on the structural properties and photocatalytic activities of solvothermal synthesized TiO2 hollow nanoparticles,” *Ceram. Int.*, vol. 40, no. 5, pp. 6441–6446, Jun. 2014, doi: 10.1016/j.ceramint.2013.11.094.

[20] J. Lv *et al.*, “Effect of annealing temperature on photocatalytic activity of ZnO thin films prepared by sol-gel method,” *Superlattices Microstruct.*, vol. 50, no. 2, pp. 98–106, Aug. 2011, doi: 10.1016/j.spmi.2011.05.003.

[21] R. Ding *et al.*, “A general solution synthesis route to ZnO-based nanorod arrays on ceramic/silicon/quartz glass/metal substrates,” *Sci. Adv. Mater.*, vol. 2, no. 3, pp. 396–401, Sep. 2010, doi: 10.1166/sam.2010.1101.

[22] Z. Zhou, Y. Zhao, and Z. Cai, “Low-temperature growth of ZnO nanorods on PET fabrics with two-step hydrothermal method,” *Appl. Surf. Sci.*, vol. 256, no. 14, pp. 4724–4728, May 2010, doi: 10.1016/j.apsusc.2010.02.081.

[23] G. Venkatesh, S. Prabhu, M. Geerthana, P. Baskaran, R. Ramesh, and K. M. Prabu, “Facile synthesis of rGO/CaSnO3 nanocomposite as an efficient photocatalyst for the degradation of organic dye,” *Optik (Stuttg).*, vol. 212, p. 164716, Jun. 2020, doi: 10.1016/j.ijleo.2020.164716.

[24] P. Arumugam, P. Sengodan, N. Duraisamy, R. Rajendran, and V. Vasudevan, “An effective strategy to enhance the photocatalytic performance by forming NiS/rGO heterojunction nanocomposites,” *Ionics (Kiel).*, vol. 26, no. 8, pp. 4201–4212, Aug. 2020, doi: 10.1007/s11581-020-03564-y.

Figures

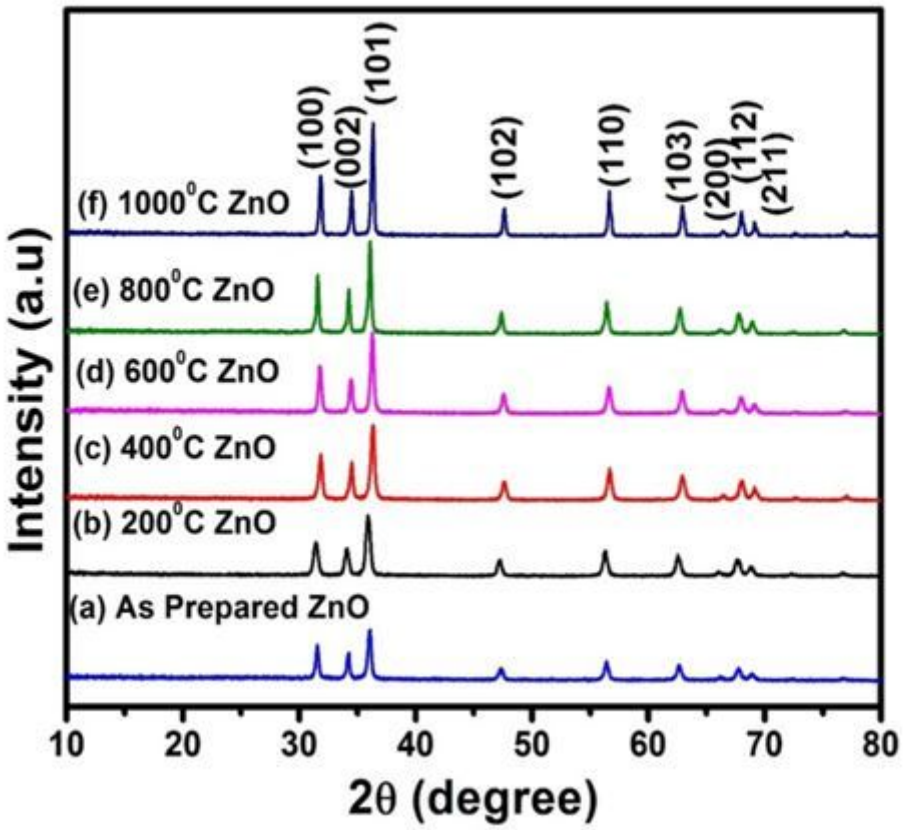

Figure 1

Powder XRD patterns of (a) ZnO, (b) 200 oC, (c) 400 oC, (d) 600 oC, (e) 800 oC and 1000 oC nanostructures.

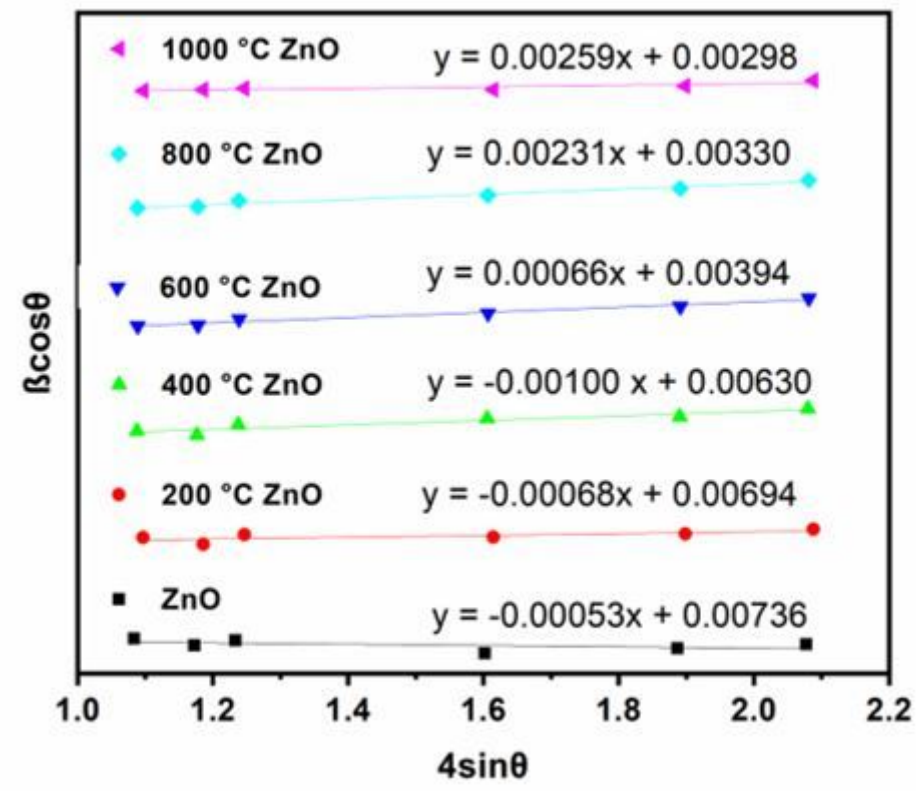

Figure 2

Williamson–Hall plots for ZnO (as-synthesized) and annealed nanostructures

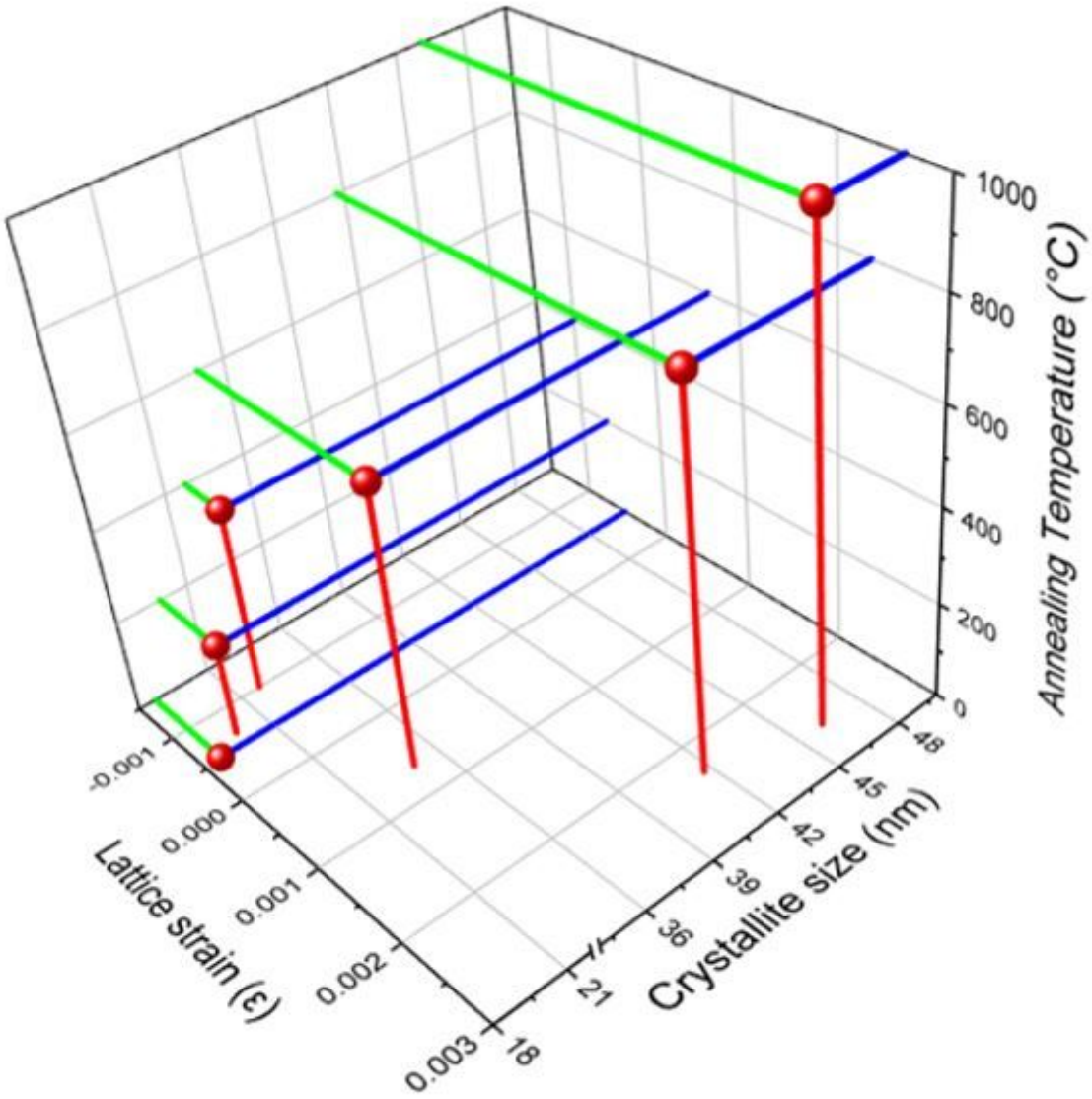

Figure 3

Plot of lattice strain vs crystallite size and annealing temperature.

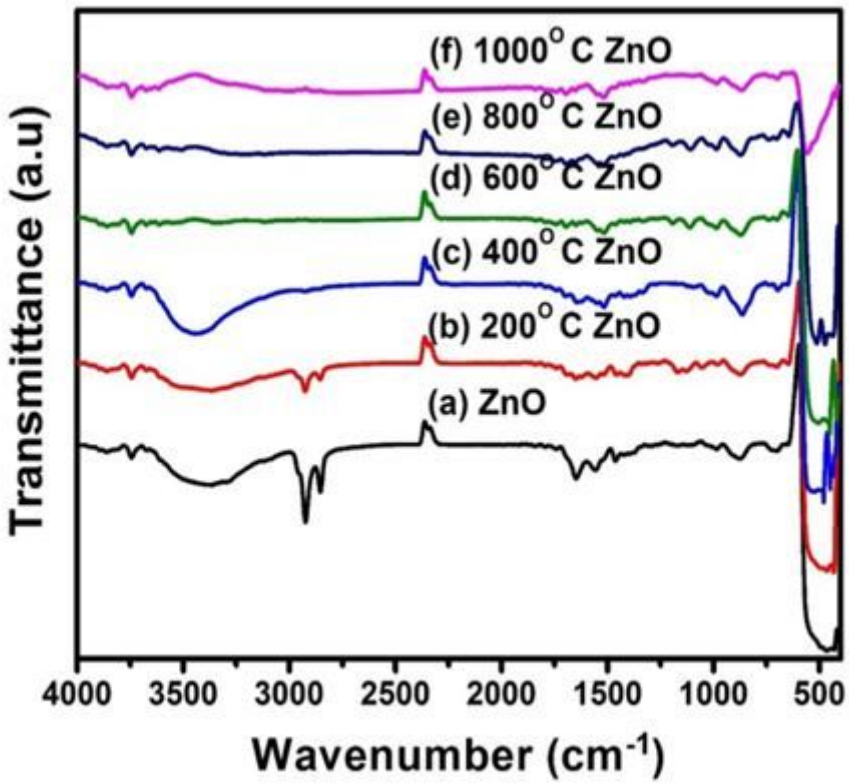

Figure 4

FTIR spectra of (a) ZnO, (b) 200 oC, (c) 400 oC, (d) 600 oC, (e) 800 oC and 1000oC nanostructures.

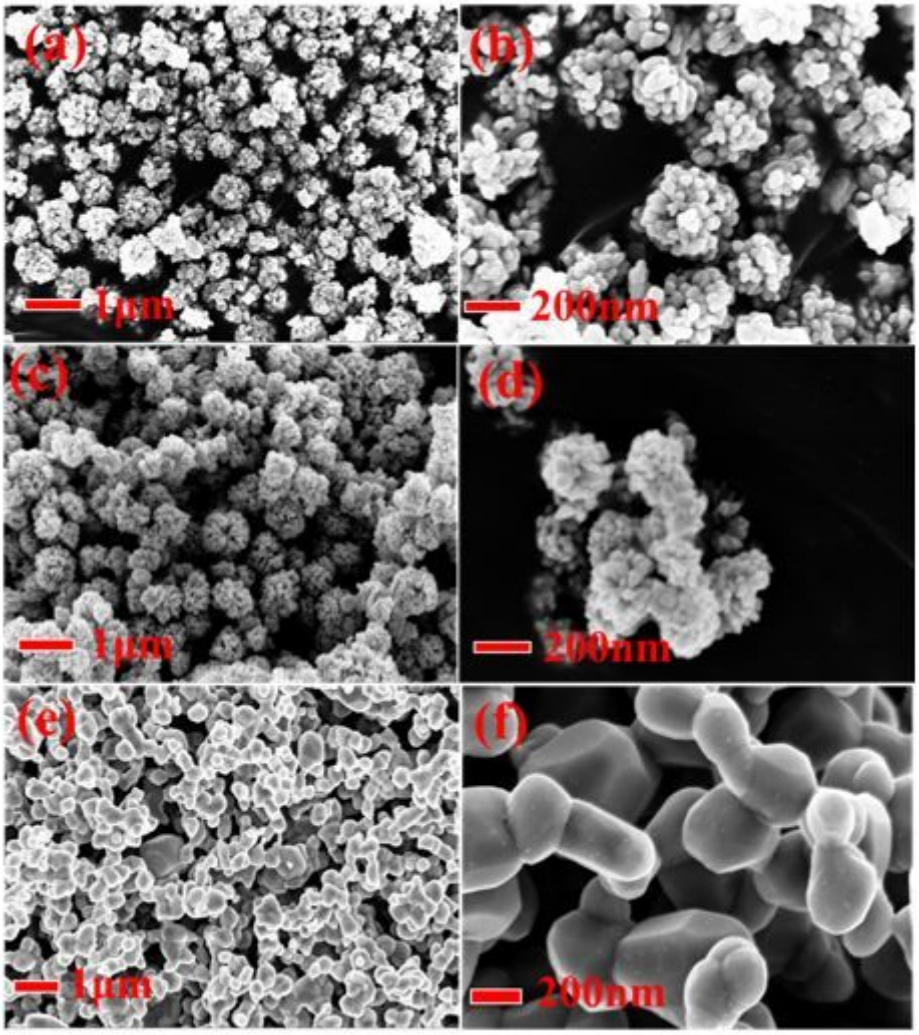

Figure 5

FE-SEM images for (a-b) as prepared ZnO, (c-d) 400oC and (e-f) 1000oC nanostructures.

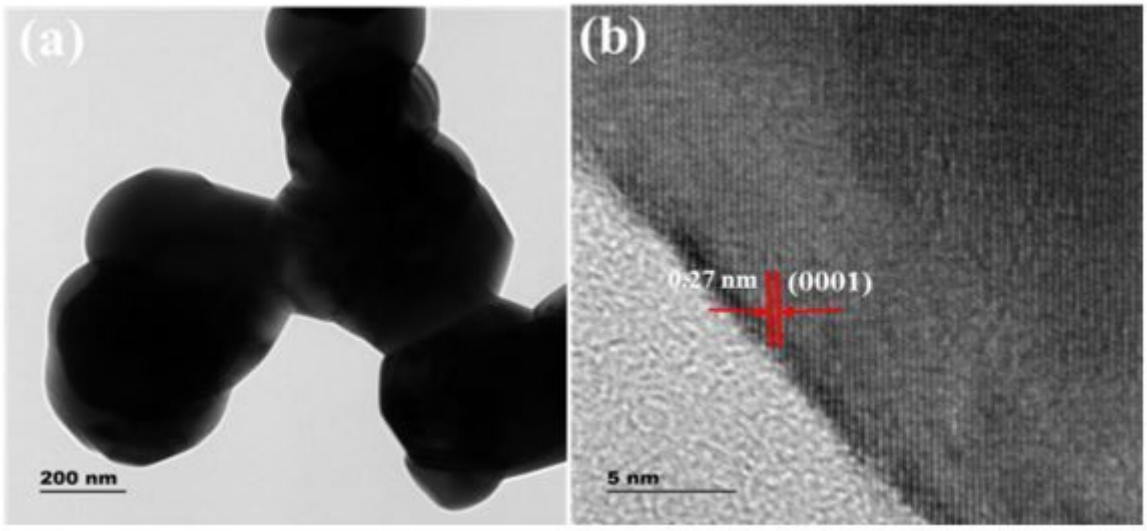

Figure 6

6(a) TEM and (b) HR-TEM images of 1000ºC ZnO nanostructure.

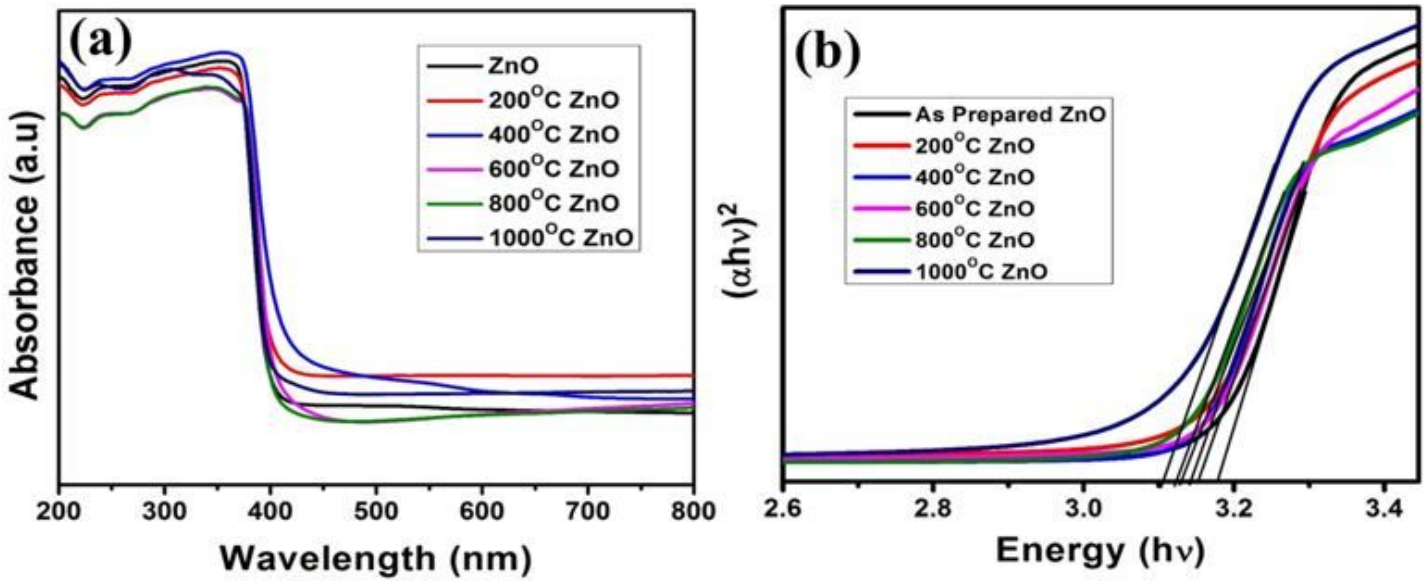

Figure 7

(a) UV- DRS Spectra and (b) band gap energy of (a) ZnO, (b) 200 oC, (c) 400 oC, (d) 600 oC, (e) 800 oC and 1000 oC nanostructures.

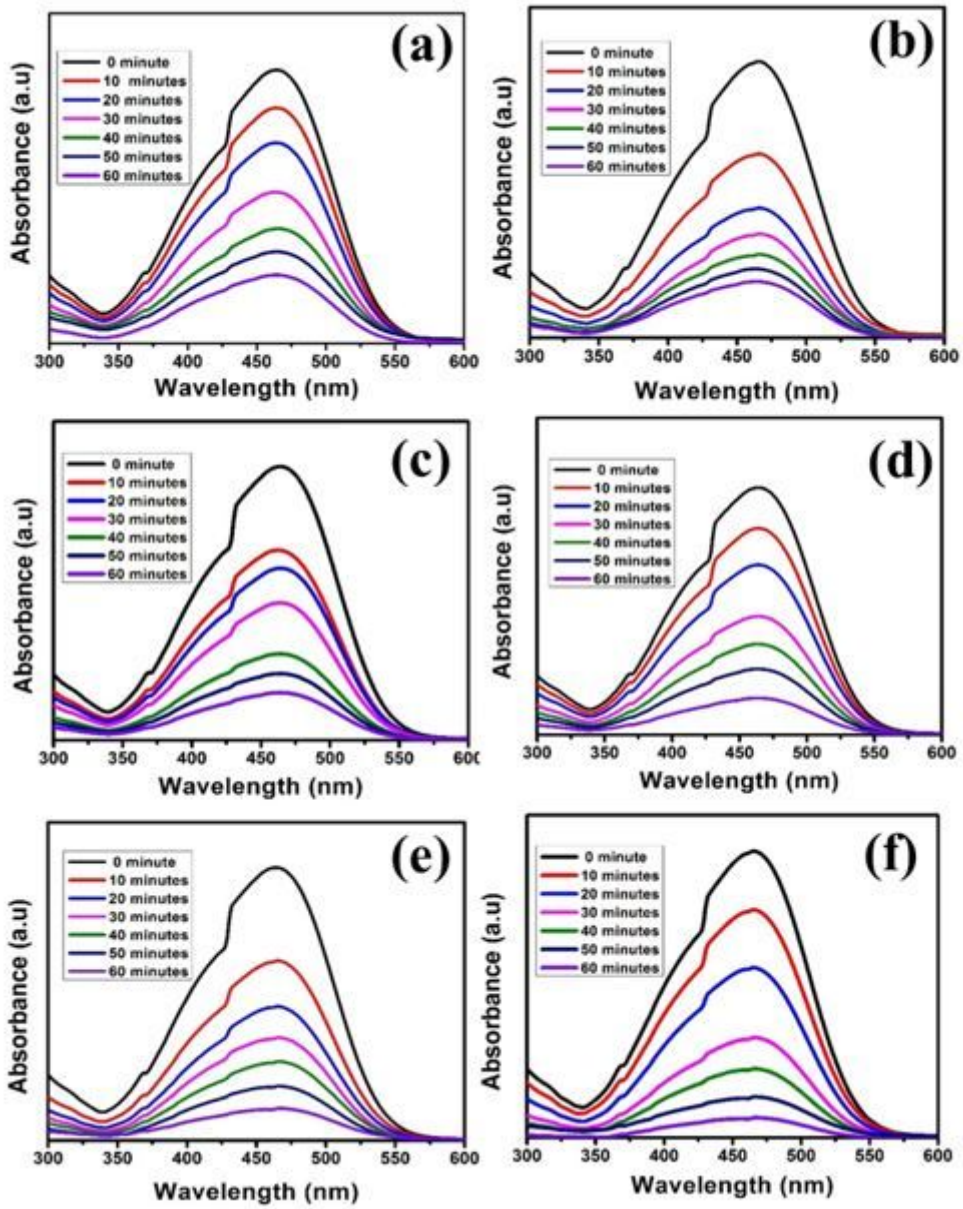

Figure 8

Photocatalytic activity of ZnO photocatalyst as a function of the irradiation time under different annealing nanoparticles.

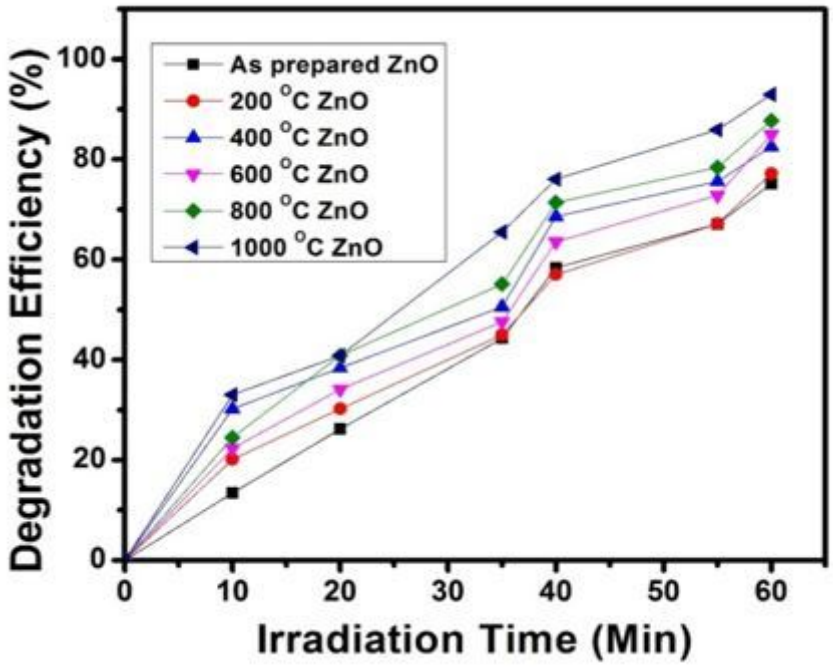

Figure 9

Degradation efficiency of ZnO photocatalyst as a function of the irradiation time under different annealing nanoparticles.

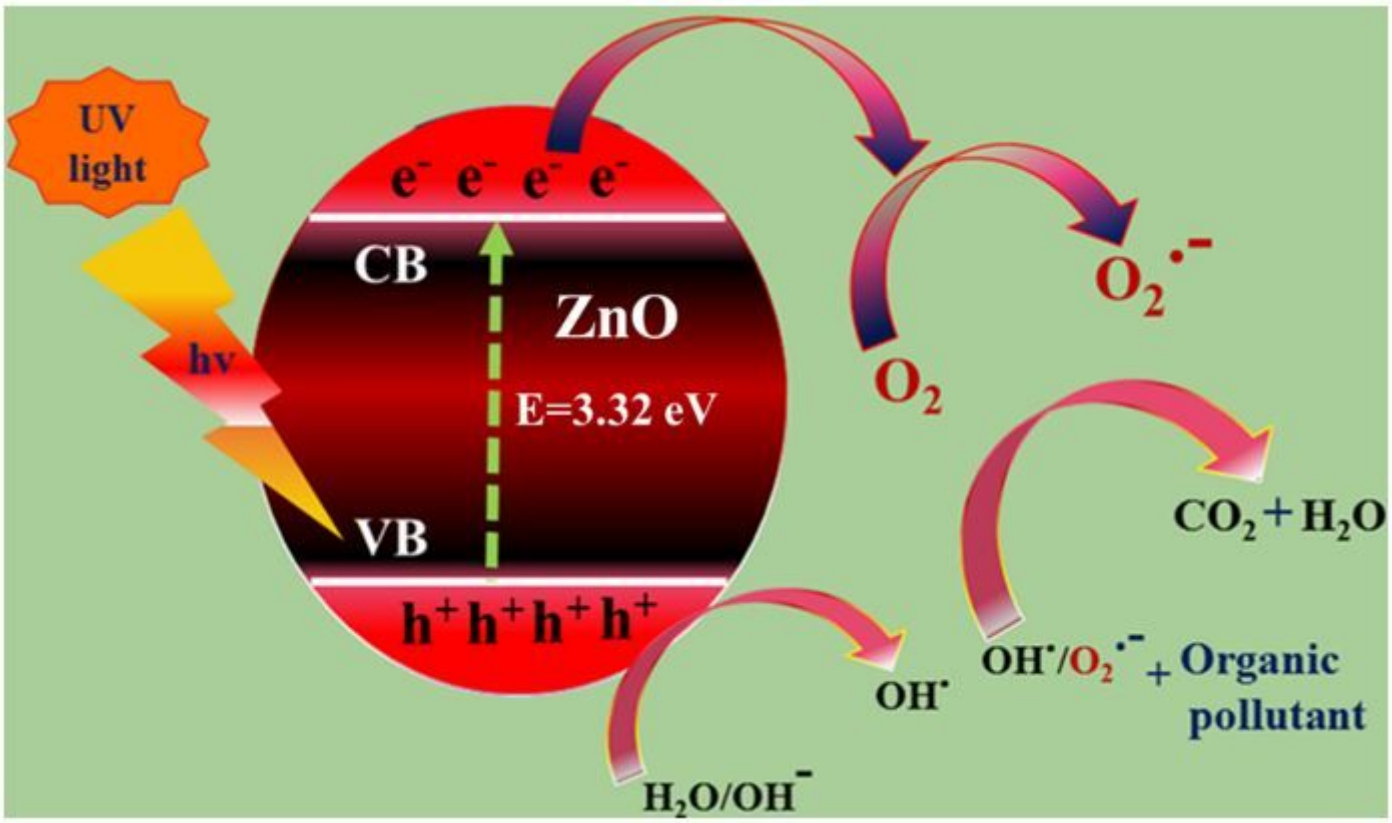

Figure 10

Schematic diagram of the photocatalytic process for ZnO nanoparticles under UV- light irradiation.

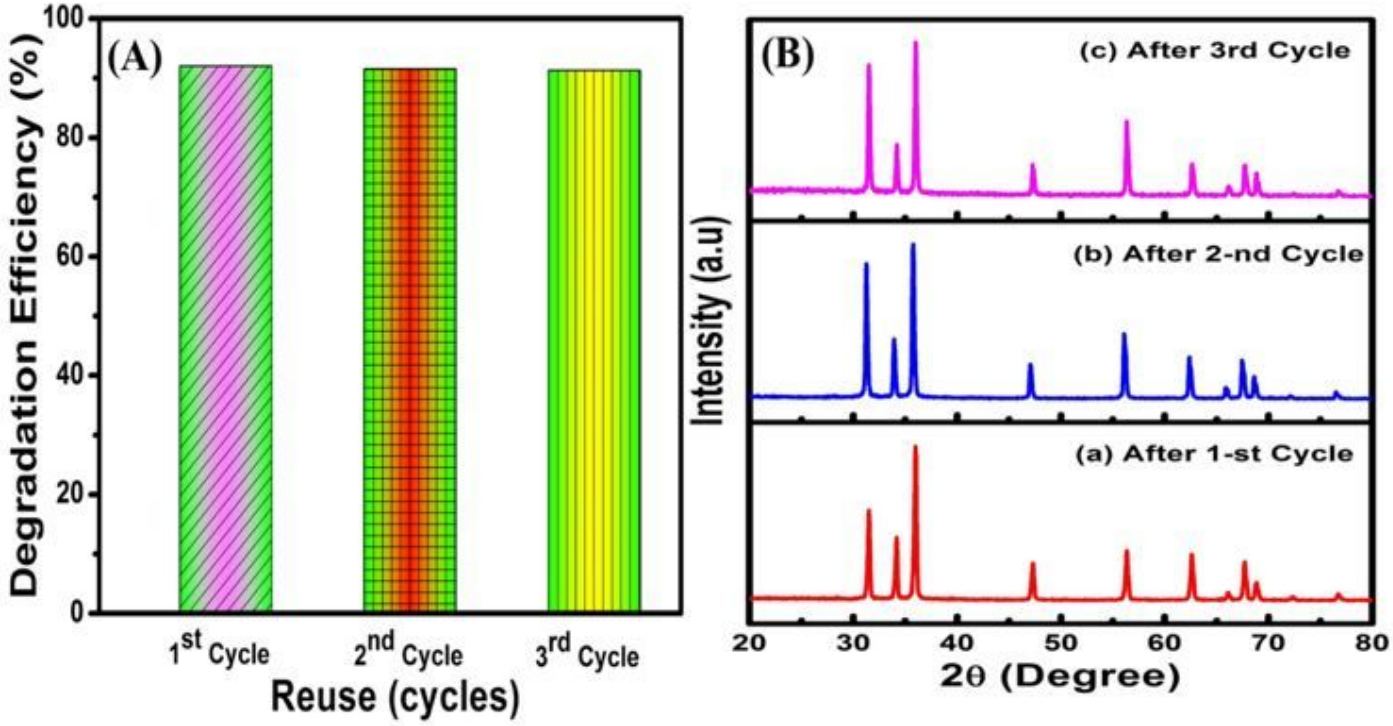

Figure 11

(A) Reusability test for 1000oC ZnO photocatalyst up to 3 cycles and (B) XRD patterns of reused 1000oC ZnO sample up to 3 cycles.